Evaluation of Anticancer Potential of N(4)-Alkyl Substituted 5-Methoxyisatin Thiosemicarbazones: Synthesis, Characterization and Molecular Docking

Upendra Chaudhary[1], Vijay Gurung[2], Sayed Tariq Pachakhan[2],
Jhashanath Adhikari Subin[3], Yuba Raj Pokharel[2,*] and Paras Nath Yadav[1,*]

[1]Central Department of Chemistry, Tribhuvan University, Kirtipur, Kathmandu 44618, Nepal
[2]Faculty of Life Science and Biotechnology, South Asian University, Akbar Bhawan, Chanakyapuri, New Delhi-110021, India
[3]Department of Chemistry, D.A.V. College, Jawalakhel, Lalitpur 44700, Nepal

*Corresponding authors: E-mail: yrp@sau.ac.in; pnyadav219@gmail.com

(Z)-N-ethyl-2-(5-methoxy-2-oxoindolin-3-ylidene)hydrazine-1-carbothioamide (MeOIstEt) and (Z)-2-(5-methoxy-2-oxoindolin-3-ylidene)-N-methylhydrazine-1-carbothioamide (MeOIstMe) were synthesized and subjected to elemental analysis and various characterization techniques *viz.* IR, ^{1}H NMR, ^{13}C NMR, UV-Vis and HRMS. The synthesized N(4)-alkyl substituted thiosemicarbazones were evaluated for their anticancer activity against various cancer cell lines like breast cancer (MCF-7), skin cancer (A431) and lung cancer (A549). In micromolar concentrations, the synthesized compounds exhibited moderate anticancer activity (IC$_{50}$, 6.59-36.49 μM). The compound MeOIstEt was found to be more effective than MeOIstMe against A549 and MCF-7 cell lines, whereas compound MeOIstMe was found to be more potent against A431 cell lines. From flexible receptor molecular docking calculations in a hydrated environment, one of the compounds showed better binding affinity than one FDA approved drug. The insights from computational studies have strengthened the experimental findings and *vice-versa*. This work demonstrates the role of multiple approaches in finding better drug candidate with efficient anti-cancer properties.

Keywords: Anticancer activity, Breast cancer, 5-Methoxyisatin, Molecular docking, Thiosemicarbazones.

INTRODUCTION

Around 13% of all fatalities worldwide every year are attributed to cancer, making it a leading cause of mortality [1]. In affluent countries, cancer is still responsible for even more than 20% of all deaths, making it an extremely high relative mortality rate. Breast cancer is among the most common chronic cancers in women and also the major cause of death [2]. The affinity of 1H-indole-2,3-diones for tyrosine kinase, cyclin-dependent kinases (CDKs) and carbonic anhydrase isozymes (CAIs) can be related to anticancer mechanism [3]. Many tyrosine and serine/threonine kinases like CDKs, FLT3 kinase, polo-like kinase 4 (PLK4), glycogen synthase kinase-3β(GSK-3β), aurora B kinase, p90 ribosomal S6 protein kinase 2 (RSK2) and microtubule affinity-regulating kinase 4 (MARK4) were identified as suitable target for inhibition by isatin derivatives [4]. According to Cane *et al.* [5] at a dosage of 0.1 mM, isatin suppressed the growth of a human promyelocytic leukemia

(HL60) cancer cell line by 80%, causing DNA fragmentation and chromatin condensation. Cancer cell lines resistant to apoptosis, including such as U373, A549, SKMEL-28 and OE21, as well as apoptosis-sensitive cells, such as HS683, MCF-7, B16F10 and PC-3, were suppressed by isatin-based hetero-cyclic compounds [6]. In U-937 cells, moderate doses of 5,6,7-tribromoisatin (4 μM) were found to be anti-proliferative, whereas high quantities (130 μM) were found to be cytotoxic [7]. The thiosemicarbazone of 1-morpholino/piperidinomethyl-5-nitroisatin was assessed 60 human tumor cell line *in vitro* on a non-small cell lung cancer cell line (HOP-62, GI$_{50}$ value -8.00) and leukaemia cell lines (HL-60(TB), GI$_{50}$ value -6.30, MOLT-4, GI$_{50}$ value -6.18) [8]. With an IC$_{50}$ of 0.9 μM, 5-fluoro-2-pyridine formamide-4-pyrrolidinyl-3-thiosemicarbazone suppressed anti-apoptotic protein Bcl-2, c-Jun, JNK, MAPK or MAP (mitogen-activated protein) kinase activation and triggering endogenous cell apoptosis in MCF-7 cells [9]. Using the MTT assay, Juranic *et al.* [10] found that isatin-β-thiocarbo-

hydrazone and N-ethylisatin-β-thiocarbohydrazone exhibited cytotoxic effects on B16 (murine melanoma), HeLa (human cervical cancer) and human peripheral blood mononuclear cell lines. N(4) substituted 5-nitroisatin-3-thiosemicarbazones were tested for their ability to inhibit urease *in vitro* and displayed a strong inhibitory effect with an IC$_{50}$ value of 16.4 μM [11]. With an *in vitro* PLA2 inhibition assay and an *in silico* molecular docking analysis, 5-methoxyisatin-3-thiosemicarbazone was explored *in vitro* antioxidant behaviour and cytotoxicity against MCF-7 (breast cancer cell line) [12]. *In vitro* antiproliferative activity of (*Z*)-2-(5-fluoro-2-oxo-indolin-3-ylidene)-*N*-phenylhydrazinecarbothioamide against human colon cancer cell line (HCT-116) with IC$_{50}$ = 31.4 μM was observed [13].

5-Methoxyisatin thiosemicarbazones derivatives were found to be effective against MCF-7, A549 and HeLa cell lines *in vitro*, with an IC$_{50}$ of 14.83 ± 0.45 μM, 17.88 ± 0.16 and 6.89 ± 0.42 μM, respectively [14]. The anticancer activity of 2-acetylpyridine N-ethylthiosemicarbazone moieties on Leukemia P388 cells were examined. Both *in vitro* and *in vivo*, there was a good correlation and effectiveness in cell division delay (*p* < 0.01) [15]. The 5-nitroisatin thiosemicarbazone derivatives displayed *in vitro* antiproliferative activity against HeLa cells with an IC$_{50}$ value of 16.52 ± 1.08 μM and considerable antioxidant activity with an IC$_{50}$ value of 7.24 ± 0.09 μM [16]. Breast cancer cells (MCF-7), epidermoid carcinoma cell (A431) and PNT2 (normal prostate epithelium cell) were tested for their susceptibilities to the *in vitro* antiproliferative effects of N(4)thiomorpholinylisatin/5-haloisatin thiosemicarbazones analogous. The compounds demonstrated cell viability values of 0.94 μM, 0.77 μM, 0.79 μM and 0.61 μM in MCF-7 cell line and 0.56 μM, 0.55 μM, 0.47 μM and 1.19 μM in A431 cell line, respectively [17].

EXPERIMENTAL

5-Methoxyisatin, 4-ethyl-3-thiosemicarbazide and 4-methyl-3-thiosemicarbazide (Alfa-Aesar), carbon disulphide (Qualigens fine chemicals), sodium chloroacetate (Chemical center, India), hydrazine hydrate, 98% (Fisher-Scientific), acetonitrile, 98% (Merck), methyl alcohol, 98% (Fisher-Scientific), ethyl alcohol, 99.9% (Merck), glacial acetic acid, 98% (Fisher-Scientific), concentrated hydrochloric acid (Merck) and sodium hydroxide (Fisher-Scientific) were used as obtained.

Melting points were measured using the Philip Harris Melting Point Apparatus. Elemental analysis was carried out using a LECO Truspec Micro analyzer at IIT Madras, India. FT-IR spectra were recorded using a Shimadzu, Tracer 100 FTIR spectrometer in the 4000-400 cm^{-1} range. SPECORD®200 PLUS UV-visible spectrophotometer was used to collect UV-Visible spectra in MeOH solutions between 600 and 200 nm. NMR spectra were recorded in DMSO-*d$_6$* using TMS as an internal standard on a Bruker Advance III HD NMR, 400 MHz spectrometer and mass spectra were recorded using ESI-HRMS on a Bruker IMPACT HD liquid chromatography mass spectrometer at the Department of Chemistry, Savitribai Phule Pune University, Pune, India.

Synthesis of N(4)-substituted thiosemicarbazones: The compounds (*Z*)-*N*-ethyl-2-(5-methoxy-2-oxoindolin-3-ylidene)-hydrazine-1-carbothioamide (MeOIstEt) and (*Z*)-2-(5-methoxy-2-oxoindolin-3-ylidene)-*N*-methylhydrazine-1-carbothioamide (MeOIstMe) were synthesized by refluxing a stoichiometric ratio of the respective thiosemicarbazide (2.82 mmol) and 5-methoxyisatin (2.82 mmol) in absolute ethanol (20 mL) and glacial acetic acid for 6 h (**Scheme-I**) [18]. The refluxed product was cooled to room temperature, filtered and washed with absolute alcohol. The product was dried and recrystallized in EtOH.

(*Z*)-*N*-Ethyl-2-(5-methoxy-2-oxoindolin-3-ylidene)-hydrazine-1-carbothioamide (MeOIstEt): Yield: 49.39%; colour: brown; m.p.: 250 ºC; Anal. calcd. (found) % for C$_{12}$H$_{14}$N$_4$O$_2$S (*m.w.* 278.33): C, 51.75 (51.65); H, 5.07 (5.04); N, 20.13 (20.05). FTIR (KBr, ν$_{max}$, cm^{-1}): 3313 (s, H-N; indole), 3257 (w, H-N; azomethine), 1683 (s, C=O), 1529 (s, C=N), 1288, 783 (s, C=S), 1139 (s, N-N), 1184 (s, -OCH$_3$). ^{1}H NMR (δ, ppm): 12.69 (s, 1H, HN-C=S & NH), 7.87 (d, 1H, C7-H), 7.75 (d, 1H, C4-H), 7.13 (d, 1H, C6-H), 3.84 (t, 2H, aliphatic-C11), 3.79 (s, 3H, -OCH$_3$), 1.35 (m, 3H, aliphatic-C12). ^{13}C NMR (δ, ppm): 177.16 (C10), 163.20 (C2), 155.75 (C5), 136.37 (C3), 132.38 (C9), 121.21 (C7), 117.62 (C8), 112.24 (C6), 106.60 (C4), 56.09 (-OCH$_3$), 39.90 (C11), 14.48 (C12). ESI-HRMS: *m/z* [Found (calcd.)]: 279.0910 (279.0910) [M+H]$^+$, 301.0733 (301.0729) [M+Na]$^+$. UV-Vis [λ$_{max}$ (nm) (MeOH)]: 358 (n-π*), 283 (π-π*).

(*Z*)-2-(5-Methoxy-2-oxoindolin-3-ylidene)-*N*-methyl-hydrazine-1-carbothioamide (MeOIstMe): Yield: 86.07%; colour: brown; m.p.: 280-282 ºC; Anal. calcd. (found) % for C$_{11}$H$_{12}$N$_4$O$_2$S (264.30): C, 49.99 (50.58); H, 4.58 (4.44); N, 21.20 (21.15). FTIR (KBr, ν$_{max}$, cm^{-1}): 3303 (s, H–N; indole), 3233 (w, H-N; azomethine), 1696 (s, C=O), 1555 (s, C=N),
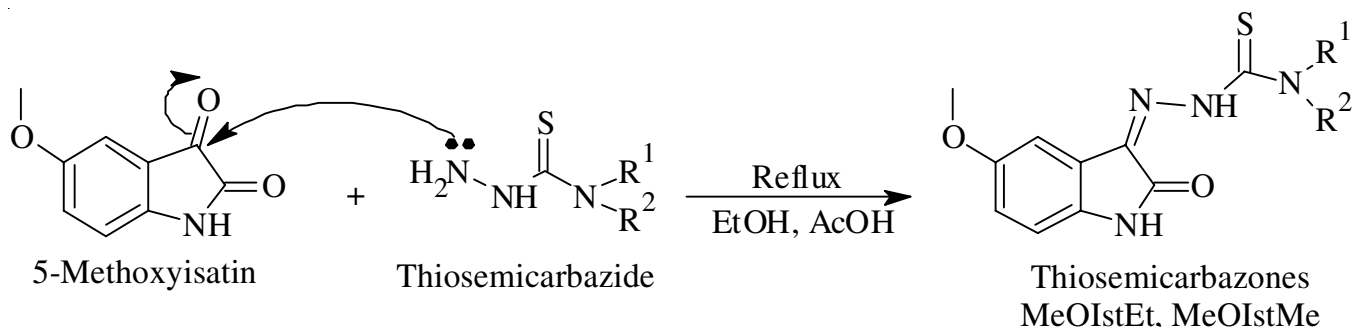
Where, MeOIstEt (R^1 = H, R^2 = -C$_2$H$_5$), MeOIstMe (R^1 = H, R^2 = -CH$_3$)

Scheme-I: Synthesis of N(4)-alkyl substituted thiosemicarbazones

1291, 744 (s, C=S), 1132 (s, N-N), 1196 (s, -OCH$_3$). ^{1}H NMR (δ, ppm): 12.58 (s, 1H, HN-C=S), 11.01(s, 1H, indole-NH), 7.25 (d, 1H, C7-H), 7.25 (d, 1H, C4-H), 6.94 (m,1H, thiourea), 6.92 (d, 1H, C6-H), 3.76 (s, 3H, -OCH$_3$), 3.35(m, 3H, aliphatic-C11). ^{13}C NMR (δ, ppm): 178.17 (C10), 163.21 (C2), 155.77 (C5), 136.41 (C3), 132.29 (C9), 121.27 (C7), 117.65 (C8), 112.27 (C6), 106.43 (C4), 56.08 (-OCH$_3$), 31.78 (C11). ESI-HRMS: m/z [Found (calcd.)]: 265.0766 (265.0753) [M+H]$^+$, 287.0569 (287.0573) [M+Na]$^+$. UV-Vis [λ$_{max}$ (nm) (MeOH)]: 356 (n-π*), 282 (π-π*).

Anticancer activity

Cell lines: A549, MCF-7 and A431 cell lines were cultured in complete DMEM media.

Cell viability assay: Cell viability of A431, MCF-7 and A549 cells were assessed by crystal violet assay. Approximately 5×10^3 cells were seeded in each well of 96 wells plate. Cells were treated with different concentration of compounds and incubated for 48 h. After 48 h, the media was discarded. Cells were stained with 80 mL (0.4%) crystal violet prepared in 50% methanol and incubated for 30 min on a bench rocker with 20 oscillations per minute. After that cells were washed by dipping in a beaker filled with tap water which prevented the washout of cells. Culture plates were kept overnight for air drying at room temperature. Next day, 150 μL of methanol was added in each well and kept on a rocker for 30 min. Finally, optical density was measured in micro-plate reader at 570 nm.

RESULTS AND DISCUSSION

FTIR studies: In FTIR spectrum of N(4) alkyl substituted thiosemicarbazones, the broad symmetric and asymmetric stretching vibration of indole N-H was observed between 3313-3303 cm^{-1} [19], whereas the N-H stretching vibration of azomethine was observed between 3257-3233 cm^{-1}. The slight shift to higher wavenumbers in indole N-H (3313 cm^{-1}) is probably a consequence of changes in hydrogen bonding. The absence of a stretching band at about 2600-2500 cm^{-1}, which specifies to ν(S-H) and the presence of two strong bands specific to ν(C=S) at 1291-1288 cm^{-1} and 783-744 cm^{-1} indicated the existence of the thione tautomer of thiosemicarbazone [20,.21]. The strong stretching bands appeared in the thiosemicarbazone at the range of 1696-1683 cm^{-1} and 1555-1529 cm^{-1}, respectively, assigned to ν(C=O) and (C=N) [22,23]. The medium stretching bands were assigned to ν(N-N) of thiosemicarbazones and appeared at 1139-1132 cm^{-1} [24]. The strong stretching bands of isatin moieties of thiosemicarbazones appeared at 1196-1184 cm^{-1}, which were assigned to ν(-OCH$_3$) [25].

NMR studies: In ^{1}H NMR (DMSO-d_6) spectra of N(4) alkyl substituted thiosemicarbazones, the signals of highly acidic H-N-C=S and indol-NH protons were observed downfield as a singlet at δ 12.58 ppm and δ 11.01 ppm in ligand MeOIstMe [12]. The N(4)-ethyl compound in which the signal was attributed to the N(3)-H at δ 12.69 ppm confirmed both by its position at lower field showing an intramolecularly hydrogen-bonded proton and by its stronger dependence on the type of the N(4) substituent [26]. This is supported by the ^{1}H NMR spectra, which shows a singular peak at δ 11.01 ppm relative

to the NH adjacent to C=S [11], but no peak at 4 ppm attributed to the S–H proton in the ligand. All the aromatic protons of isatin moiety were seen as doublet signals at δ 7.25 to 6.92 ppm in the ligand, respectively. Similarly, in case of N(4) ethyl group (MeOIstEt), the signals of -CH$_2$ protons were found as a triplet at δ 3.84 ppm and the signals of -CH$_3$ protons were found as multiplet at δ 1.35 ppm [27] and N(4) methyl group (MeOIstMe), the signals of -CH$_3$ protons were found as multiplet at δ 3.35 ppm [28]. The signals of secondary amine of N(4)-H in ligand MeOIstEt was observed as singlet at δ 7.16 ppm whereas the signals of secondary amine of N(4)-H in ligand MeOIstMe was observed as singlet at δ 6.94 ppm [29]. The signals of methoxy (-OCH$_3$) protons were observed as a singlet at δ 3.79-3.76 ppm in the ligand [30].

The ^{13}C NMR spectra of the synthesized compounds were obtained in DMSO-d_6. In compounds, the –C=S (C10) signals were observed at the range of δ 178.17-177.16 ppm. The characteristic –C=O (C2) and –C=N (C3) peaks were observed at the range of 163.21-163.20 ppm and 136.41-136.37 ppm in thiosemicarbazones, respectively [31]. The aromatic carbons (C4–C9) of the isatin ring were observed at 106.60-106.43 (C4), 155.77-155.75 (C5), 112.27-112.24 (C6), 121.27-121.21(C7), 117.65-117.62 (C8) and 132.38-132.29 ppm (C9) in the thiosemicarbazones, respectively [32]. The C5 carbons atom shifted downfield due to the presence of methoxy group. The signals in N(4)-methyl group (MeOIstEt) carbons atoms (C12) were observed at 14.48 ppm and methylene group (-CH$_2$) carbon atom (C11) were observed at δ 39.30 ppm [33]. The signals of N(4) methyl group (MeOIstMe) carbon atoms C11) were seen at δ 31.78 ppm. The signals of methoxy (–OCH$_3$) carbons atoms peak was observed at δ 56.09-56.08 ppm in both the thiosemicarbazones [34].

ESI-HRMS studies: The molecular ion peaks of the proposed molecular structures were in consistent. The protonated and alkali adduct molecules were seen in the positive mode of the ESI-HRMS investigations for the mass spectral peaks of the compounds. The protonated molecular ion [M+H]$^+$ peaks obtained from thiosemicarbazones were observed at m/z = 279.0910 (calcd., 279.0910) (MeOIstEt) and m/z = 265.0766 (calcd., 265.0753) (MeOIstMe) [14]. Besides protonated peaks, the thiosemicarbazones showed the molecular ion [M+Na]$^+$ peaks: m/z = 301.0733 (calcd. 301.0729) (MeOIstEt) and m/z = 287.0569 (calcd. 287.0573) (MeOIstMe). The significant peaks at m/z 247.1185 (calcd. 247.2961) [C$_{11}$H$_{11}$N$_4$SO + H]$^+$ ion and m/z 226.9515 (calcd., 226.2754) [C$_9$H$_{11}$N$_3$O$_2$S + H]$^+$ ion were observed due to the fragment with the loss of OCH$_3$ group (m/z 31 amu) and C$_2$N group (m/z 38 amu), respectively [35].

UV-Vis studies: In MeOH, UV-visible spectral data of the compounds were recorded in the 600-200 nm region. The compounds showed two broad absorption bands with different intensity and a shoulder-like appearance in the region around 282 nm and 356 nm, which were attributed to n→π* intraligand electronic transitions, namely the bands due to the electronic transition of azomethine (-C=N), carbonyl (-C=O) and the (-HN-C=S) group [21,36]. Due to transitions of π→π* and n→π*, the electronic spectra of these compounds revealed exceptional absorption bands in the aromatic ring (C=C) and

thiosemicarbazone (C=S) and imine (CH=N) region [37]. The bands at around 356 nm were attributed to the electronic transition n→π* of the thiosemicarbazone moiety (C=S) and the bands at around 282 nm were allocated to the electronic transition π→π* of C=O on aldehyde group [18].

Biological activity: The cell viability *in vitro* of the synthesized compounds MeOIstEt and MeOIstMe was investigated at concentrations ranging from 1 to 100 µM and found to be greater than 50%. Therefore, the compounds showed modest anticancer activity against MCF-7 (breast cancer), A549 (lung cancer) and A431 (skin cancer) cells. The compound MeOIstEt was found to be the most potent proliferation inhibitor against the A549 and MCF-7 cells than MeOIstMe whereas compound MeOIstMe was found to be more potent proliferation inhibitor towards A431 cells than MeOIstEt.

Computational method and materials

Density functional theory: The quantum mechanical calculations in the framework of density functional theory (DFT) as implemented in an open-source software suite, CP2K was used [38]. The molecular geometry of the studied compounds was calculated and the models were proposed for molecular docking studies. BFGS optimizer was employed in locating the global minima of the molecules. Localized basis sets (DZVP-MOLOPT-SR-GTH) and exchange-correlation functional (BLYP) were used with 300 Ry cutoff of kinetic energy in minimizing the molecular structure up to the energy convergence of 1.0×10^{-6} Ry and the force convergence (MAX and gradient) of 1.0×10^{-4} Ry/Bohr.

Molecular docking: ADFR suite was used in accessing the best docked pose of the small molecules with the receptor proteins [39]. The active site was located by an option in the molecular docking program and also from the protein database. In some cases, CASTp server results were also considered for unanimous inferences [40]. The number of independent GA searches were set to 50 with each using up to 10,000,000 evaluations of the scoring functions. This high value ensured that the chances of capturing the best possible docked pose was maximized and instead of local minima of the scoring function, a global minima was reached in a solvated environment. The water map setting with the default weight of 0.60 and entropy of -0.20 were chosen for hydrated docking. The amino acids residues (up to 15) of the receptors at the orthosteric site were assigned to be flexible and the small molecule possessed rotational degrees of freedom during the docking process by default. The box sizes for different proteins had large variations depending upon the size of the active site. The largest box of size 22 × 28 × 19 points was chosen for the protein with PDB ID of 7BJ6 as an example. The padding of 2.00, grid spacing of 0.375 Å and smoothing of 0.500 were adopted for all the receptors.

Different clusters of docking results related to different searches were obtained and the pose with best affinity was taken for further analysis. The reference ligand was not provided and consequently the RMSD value of each distinct output was not obtained. As a representative case, one of the receptors with its active site occupied by a small molecule ligand is depicted in Fig. 1.
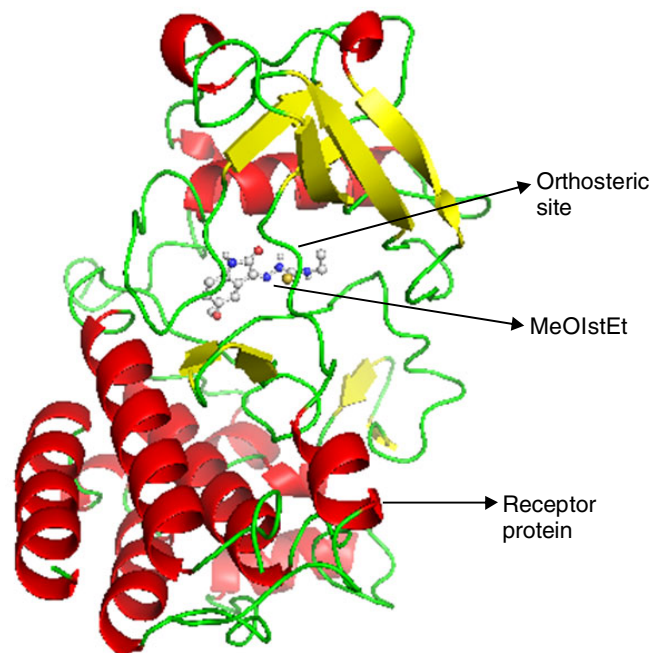
Fig. 1. Cartoon representation of a docked pose of MeOIstEt in the active site of protein with PDB ID: 4ASD (carbon gray, nitrogen blue, oxygen red, sulfur yellow, hydrogen cream spheres)

Target proteins: Various proteins represented as different PDB ID as receptors of the ligands are presented in Table-1. The search for alternate prophylactics of cancerous cell addressing different types of growth factors and other enzymes were considered for spanning a broad range of possible targets. Here, *in silico* approach addresses targeted therapy that deals with the treatment of specific cancer by obstructing the pathways or mutations causing tumor cell proliferation. The receptor with maximum amino acid residue count of 1014 and minimum of 98 were used in this work and the PDB structures were retrieved

TABLE-1			
DETAILS OF DIFFERENT KINDS OF RECEPTORS USED IN MOLECULAR DOCKING			
PDB ID	Receptor class	Feature	Overall quality factor (Disallowed %)
4ASD	VEGFR2	A monomer with 353 residues	98.64 (0.4%)
3MJG	PDGFR	A hetero-4-mer with 922 residues	82.25 (0%)
3MJK	PDGF precursor	A homo-2-mer with 1014 residues	85.96 (0%)
7BJ6	MDM2 protein	A monomer with 98 residues	100.00 (0%)
2VTA	Cyclin dependent kinase 2	A monomer with 298 residues	88.02 (0%)
3VHE	VEGFR2 kinase domain	A monomer with 359 residues	97.25 (0%)
6LVK	FGFR3	A monomer with 626 residues	98.49 (0%)

from RCSB website (rcsb.org) [41]. The protein structures were cleaned by removing water molecules, ions, metals, ligands and other small molecules. The polar hydrogens were added along with Gasteiger charges.

4ASD is a vascular endothelial growth factor receptor (VEGFR2) with 353 residue count. It is a protein tyrosine kinase receptor that regulate tumor-induced blood vessels formation. 3VHE is a similar target with 359 residue count. 3MJG is a platelet-derived growth factor receptor (PDGFR) and is involved in the development of different types of cancerous cells [42]. Its antagonist could be a good therapeutic candidate. 3MJK is a protein associated with platelet-derived growth factor precursor with 1014 residues. Only A and B chains were considered for molecular docking. 7BJ6 is a murine double minute 2 protein and is considered vital in p53 regulation and cancer cell suppression. 2VTA has been top ranked (fit score of 2.488) by an online program PharmMapper (http://59.78.96.61/ pharmmapper) [43] as potential target (cell division protein kinase 2) in cancer treatment. It consists of a single chain with 298 residues and ligands based on its docking have been currently subjected to clinical trials [44]. 6LVK is a fibroblast growth factor receptor 3 used in specially the therapeutics of bladder cancer has been shown to have significant results over VEGFR2 proteins [45]. This protein is a monomer with 626 residues. These target proteins were selected from different domains and class to encompass broad spectrum in the development of therapeutics against different types of cancer by computational methods. The evaluation of protein structure was performed by Protein Structure Analysis and Verification Server [46] using ERRAT [47] and PROCHECK [48] programs. The results showed acceptable quality of the deposited structures that could be used for molecular docking studies without any additional corrections or modifications.

Test compounds and control drugs: Thiosemicarbazones and their derivatives are nitrogen and sulfur containing compounds having diverse biological and therapeutic values [49]. Herein, specifically their anticancer potentials have been explored by using computational methods. The molecular

structures (ball and stick models) of these two compounds obtained from DFT calculations are shown in Fig. 2. In order to compare the performances of the test compounds, some FDA drugs (imatinib, ruxolitinib and lenalidomide) have also been considered as references [50]. The structures were optimized by molecular mechanics using conjugate gradient algorithm with Newton's method as line search technique. Universal force field was used for the atoms with energy convergence of 10^{-7} units. The molecular structures were obtained as PDB files and the minimization was performed by Avogadro software [51] without any constraints. Their druglikeness, pharmacodynamics and pharmacokinetics have also been studied by computational methods. Imatinib and ruxolitinib are anticancer drugs of class tyrosine kinase inhibitor (antineoplastic agent). Lenalidomide is an immunomodulatory drug used in the treatment of various types of cancer and is an angiogenesis inhibitor.

Computational resources: All the codes used were open-source software in this computational work. The visualization and interpretation were also performed using free software (Avogadro and PyMol) easily available in the internet [51,52]. A multi core Intel CPU machine with 256 GB of memory and 6 TB of storage was used in the calculations. The operating systems were Ubuntu 20.04 and Windows 8.1.

Druglikeness and pharmacology studies: In order to determine the druglike properties and for ADMET prediction of the test compounds, various parameters were calculated using ADMETlab 2.0 server [53]. The physico-chemical properties are shown as radar plots in Fig. 3 and are self-explanatory. All the parameters lie within the acceptable range (between upper and lower limits) and Lipinski's rule of five is not violated. This verifies the druglikeness and acceptable oral bioavailability.

The different parameters show that the test compounds do not possess extreme toxicity and have moderate ADME profile (Table-2). This suggests that these compounds could be used as potential drug candidates with caution (carcinogenicity and respiratory toxicity) in further clinical trials.

Anticancer properties by graph based signatures: In order to find biologically active compounds having anticancer

(a) (b)
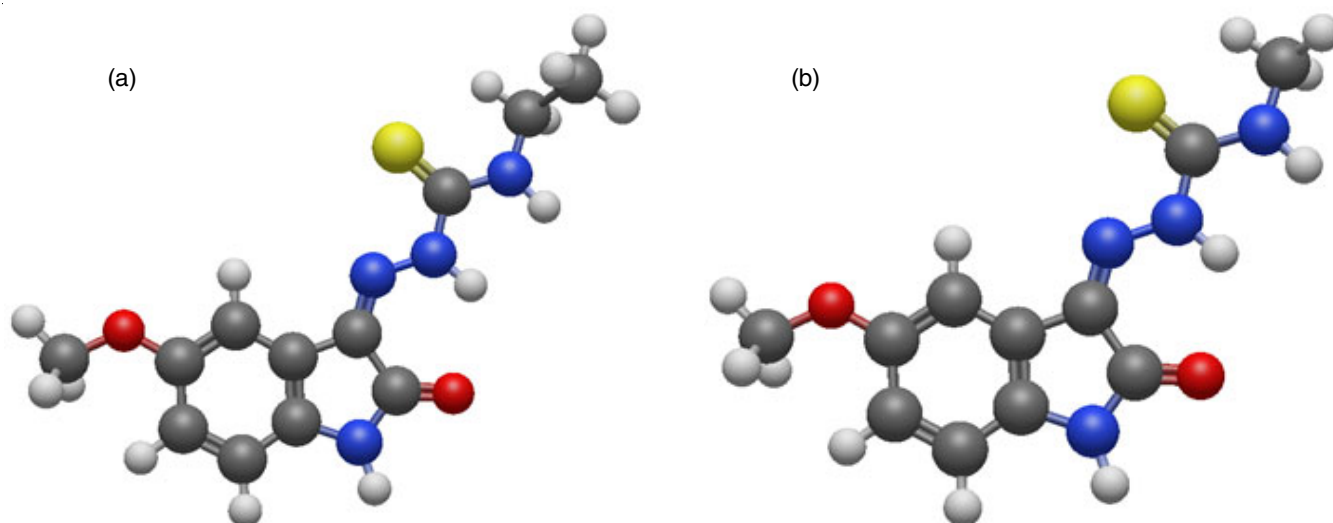
Fig. 2. Geometry optimized molecular structure of (a) MeOIstEt and (b) MeOIstMe (oxygen in red, carbon in gray, sulfur in yellow, nitrogen in blue and hydrogen in shaded white)
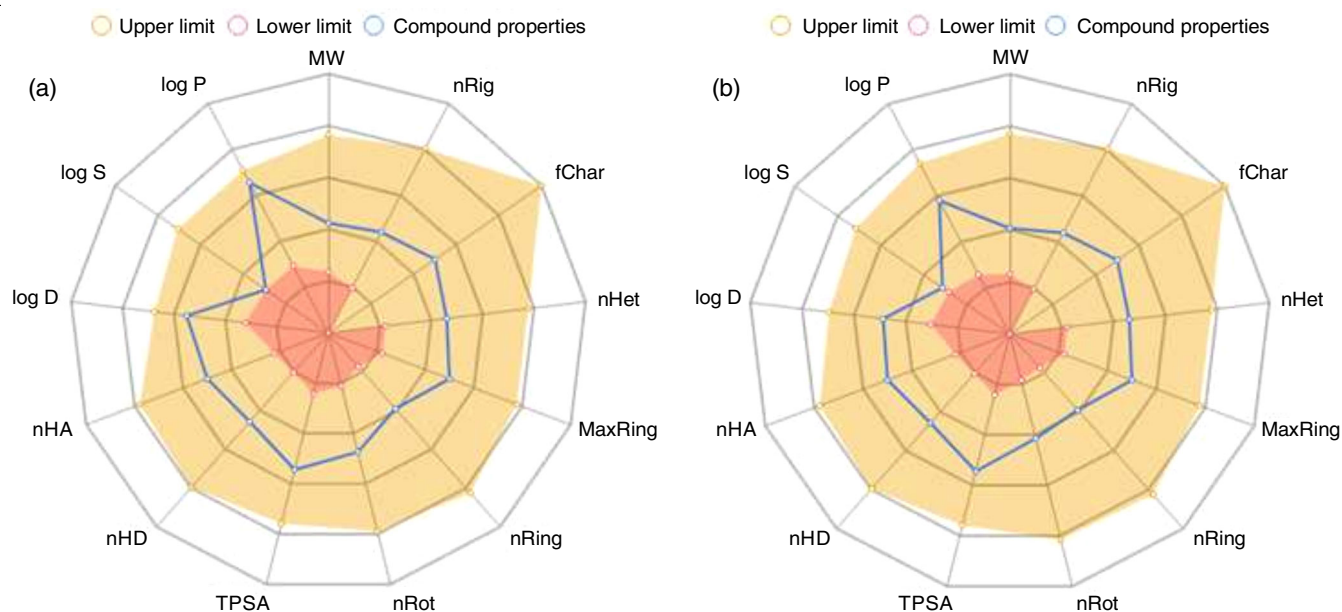
Fig. 3. Radar plots of (a) MeOIstEt and (b) MeOIstMe showing physico-chemical data

TABLE-2 SELECTED PROPERTIES PERTAINING TO ADSORPTION, DISTRIBUTION, METABOLISM, EXCRETION AND TOXICITY OF THE DRUG CANDIDATES		
Properties	MeOIstEt	MeOIstMe
Adsorption		
Caco-2 permeability (log cm/s)	-4.78	-4.90
Pgp-inhibitor	Very low probability	Very low probability
Pgp-substrate	Very low probability	Very low probability
Human intestinal absorption	10% probability	10% probability
Distribution		
Plasma protein binding	0.999	0.995
VD (L/Kg)	3.84	1.34
BBB Penetration	Low	Low
Metabolism		
CYP1A2 inhibitor	High	High
CYP1A2 substrate	High	High
CYP2C9 inhibitor	Medium	Medium
CYP2C9 substrate	High	High
Excretion		
Clearance (mL/min/Kg)	5.95	7.26
$T_{1/2}$	Long	Long
Toxicity		
HERG blockers	Low probability	Low probability
Human hepatotoxicity	70% probability of being toxic	70% probability of being toxic
AMES toxicity	Low probability	Low probability
Skin sensitization	Low probability	Low probability
Carcinogenicity	High probability	High probability
Eye irritation	Low probability	Low probability
Respiratory toxicity	High probability	High probability

capability, an online program pdCSM (http://biosig.unimelb. edu.au/pdcsm-cancer) was used [54]. The smiles notations of the test compounds were taken for job submission and no actual three dimensional molecular geometry were required. The graph based signatures as implemented in the algorithm predicts the anticancer activity (GI_{50}) against 74 cancer cell lines.

It was found that the test compound MeOIstEt was active against breast (MCF-7, MDA-MB-468), leukemia (K-562, P388-ADR), ovarian (OVCAR-4), renal (SN12K1) and small cell lung (DMS-273) cancer cell lines. For MeOIstMe, breast (MCF-7, MDA-MB-468, T47D), leukemia (CCRF-CEM, K-562, P388-ADR), ovarian (OVCAR-3, OVCAR-4), renal (SN12K1) and small cell lung (DMS-273) cancer cell lines. Surprisingly, the second compound showed activity in larger number of cases than the first compound despite having lower molecular weight.

It was found that MeOIstEt is a potent CDK2 inhibitor with IC_{50} of less than 10 µM and with pKi of 6.11 (CDK2-ligand binding affinity) from kinCSM predictor (https:// biosig.lab.uq. edu.au/kin_csm/). MeOIstMe is also a potent CDK2 inhibitor with IC_{50} of less than 10 µM and with pKi of 6.099. These findings suggest that the test compounds possess notable anticancer properties that is worthy of further investigation. Fragmentation of molecules that affects protein phosphorylation is studied by this online program and it has been found that the potential type of inhibition is type I for both the compounds.

Flexible receptor molecular docking: The data obtained from the flexible receptor molecular docking in hydrated environment of two test molecules and three approved drugs (controls) on to various proteins are tabulated in Table-3. In almost all the cases, the control drugs showed better binding affinities than the two thiosemicarbazones (MeOIstEt and MeOIstMe). Only in case of the receptor with PDB ID: 2VTA, MeOIstEt showed better binding affinity than lenalidomide. In comparing the binding affinities of MeOIstMe with that of MeOIstEt, it can be inferred that the former almost always results in weaker binding and thus may not be distinctly favoured in the inhibition of protein functioning. Apparently, the molecular weight of ligand seems to be a major factor in deter-

TABLE-3
BINDING AFFINITIES (kcal/mol) OF VARIOUS CHEMICAL COMPOUNDS AND DRUGS
AGAINST DIFFERENT RECEPTOR PROTEINS (PDB ID) RELATED TO MALIGNANT TUMORS

	m.w.	4ASD	3MJG	3MJK	7BJ6	2VTA	3VHE	6LVK
MeOIstEt	278.33	-8.8	-8.2	-7.4	-6.8	-9.7	-8.7	-8.2
MeOIstMe	264.30	-8.7	-8.1	-7.4	-6.5	-9.1	-8.5	-7.9
Imatinib	493.60	-15.7	-14.9	-9.0	-11.1	-13.1	-13.9	-13.2
Ruxolitinib	306.40	-10.6	-10.1	-8.7	-8.8	-11.4	-10.4	-9.7
Lenalidomide	259.26	-9.7	-9.2	-8.2	-7.8	-9.2	-9.2	-8.4

mining the interaction strength with the amino acid residues with the minor ones being the type, proximity and frequency of non-covalent interactions. A thorough analysis at the atomic level would ultimately provide an exact description of the inherent phenomenon.

Interactions at the atomic-level: The frequency and proximity of different types of non-covalent interactions between the amino acid residues at the orthosteric site of the protein and the docked ligand determines the strength of the protein-ligand complex. Better binding results in a stable complex and

the protein would be effectively inhibited resulting in the treatment of the disease. Hence, the pose of the ligand that forms strong bonding with the residues is the ultimate quest in structure-based drug design strategy [55] that is cost effective. Many drugs have been discovered using this technique and have circumvented the expensive experimental high-throughput screenings [56]. The receptor flexibility incorporated into the calculation along with that of the ligand's provides the closest resemblance to the realistic models as in biological systems. Fig. 4 shows the best docked pose of MeOIstEt at the active

(a)

(b)

(c)

Interactions

van der Waals	Pi-Anion
Attractive charge	Alkyl
Conventional hydrogen bond	Pi-Alkyl
Unfavourable donor-donor	Covalent bond

(d)

Interactions

van der Waals	Alkyl
Conventional hydrogen bond	Pi-Alkyl
Carbon hydrogen bond	

(e)

Interactions

van der Waals	Pi-Sigma
Unfavourable bump	Alkyl
Conventional hydrogen bond	Pi-Alkyl
Unfavourable acceptor-acceptor	
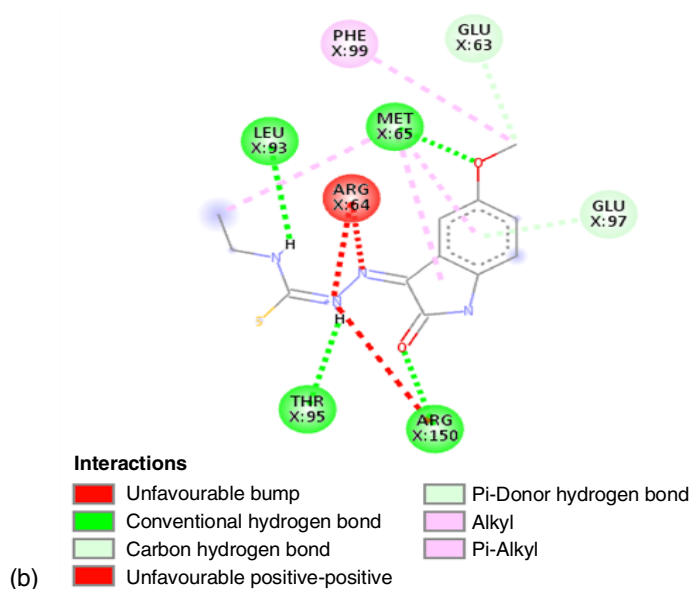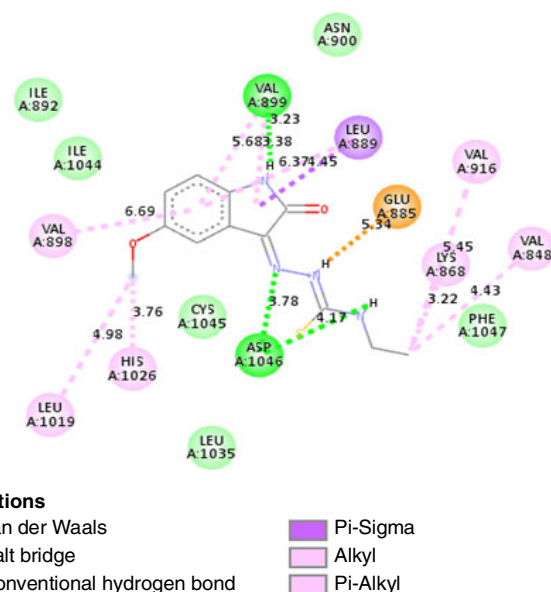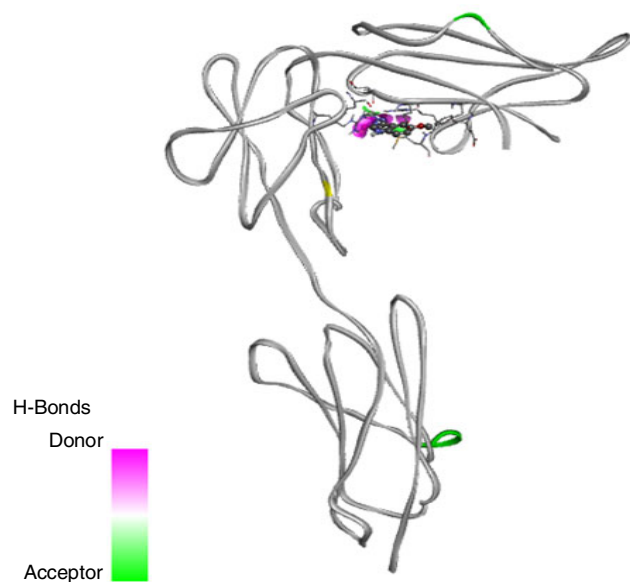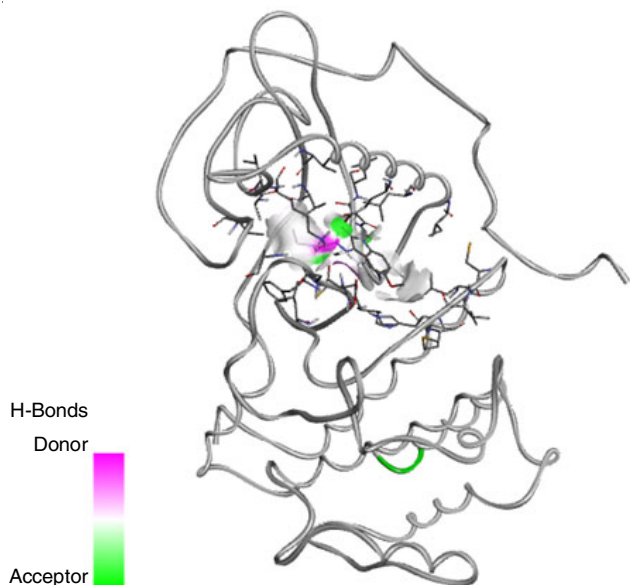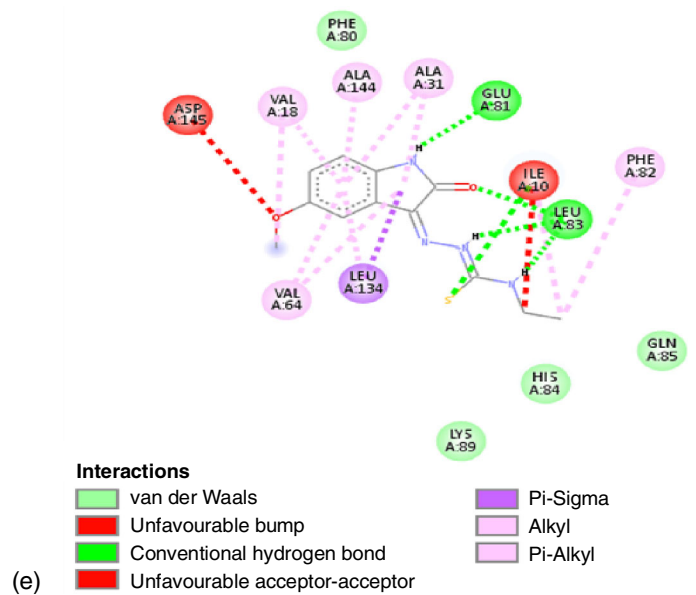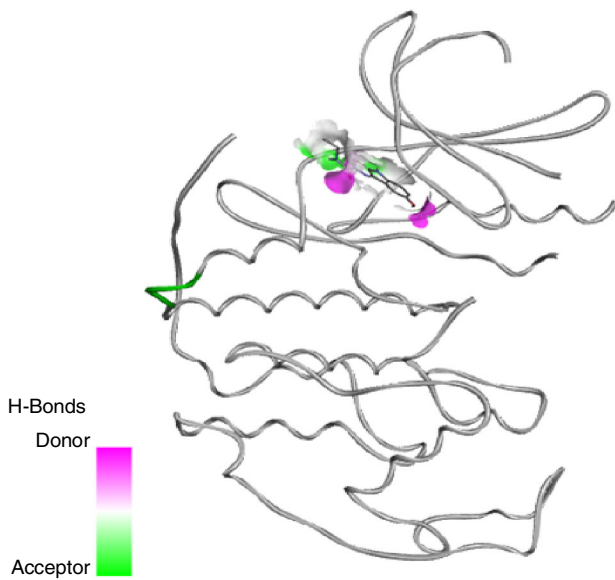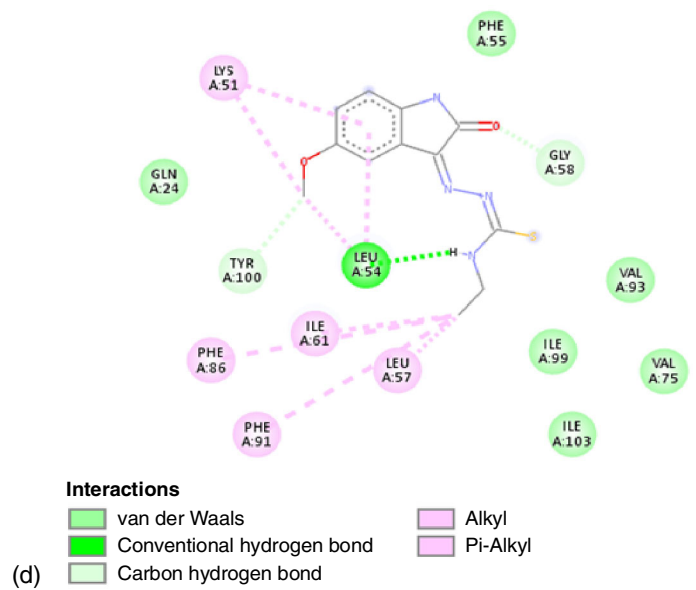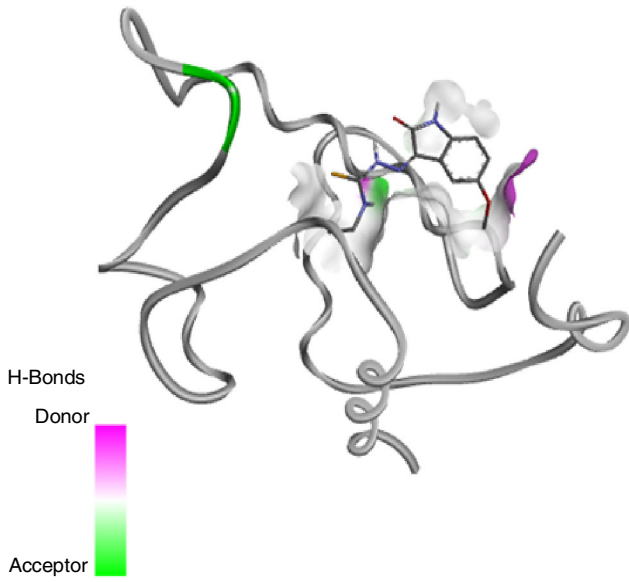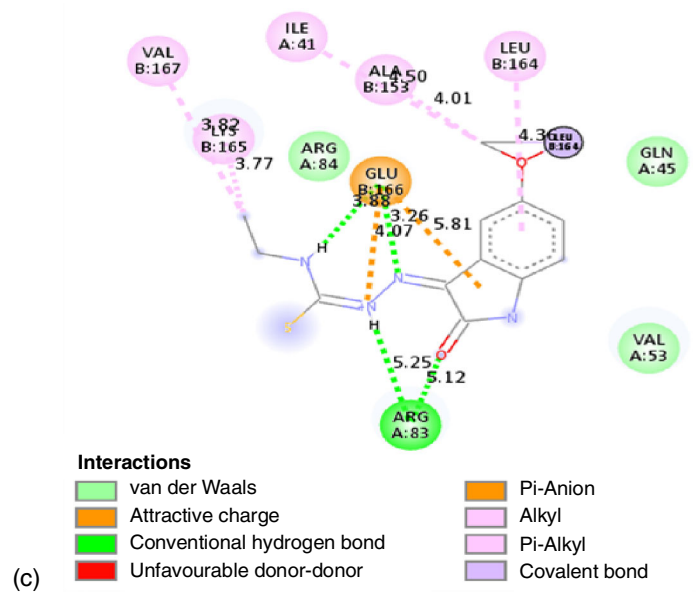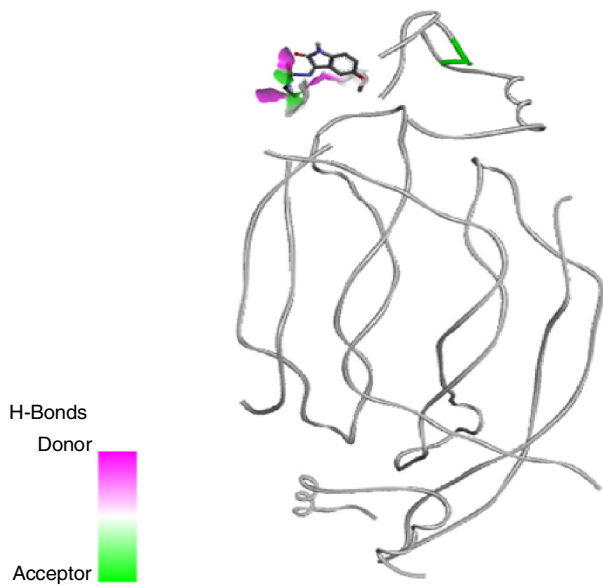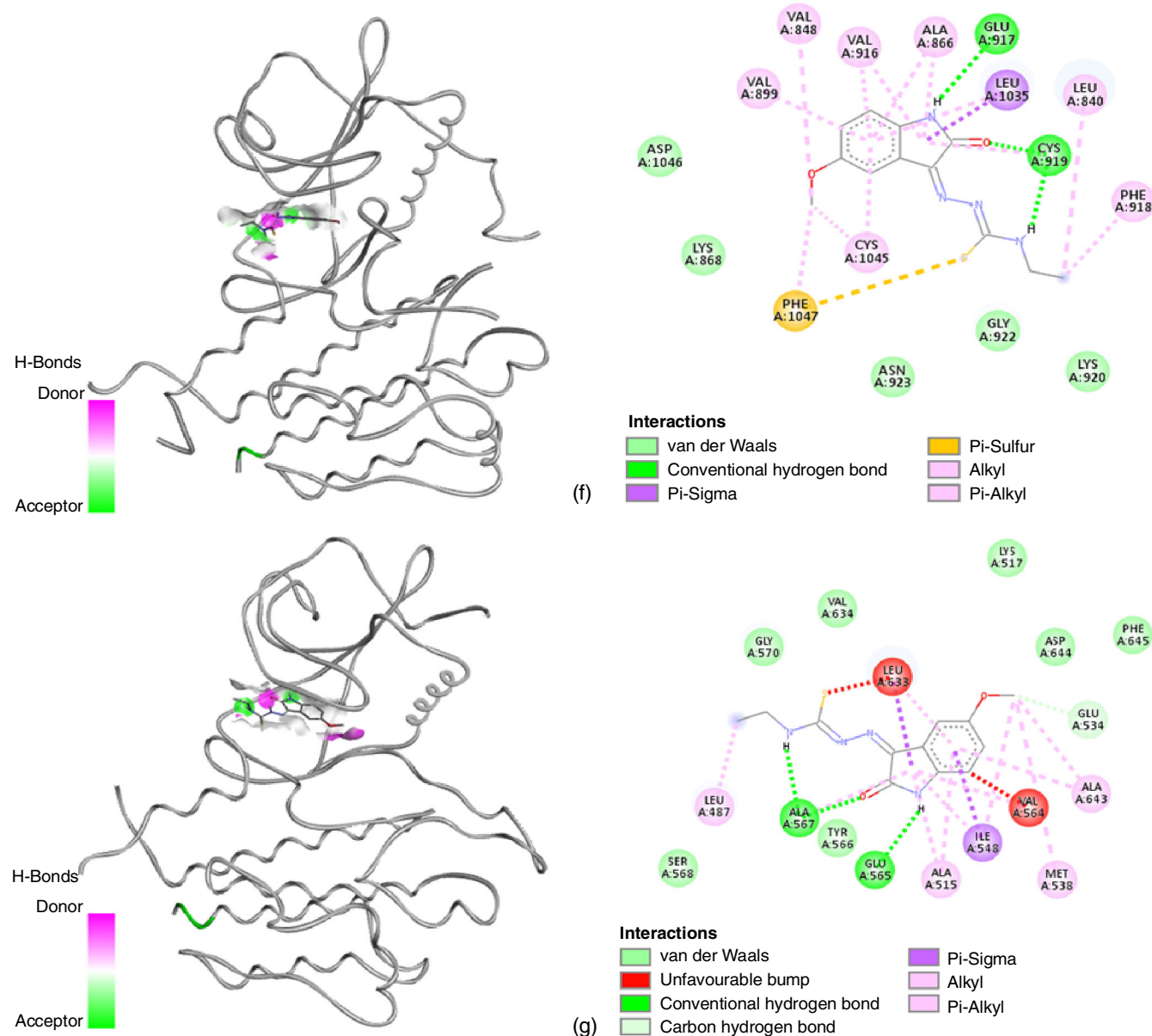
Fig. 4. 3D Plots with H-bond surface and 2D plots of Best docked pose of MeOIstEt with 4ASD (a); with 3MJG (b); with 3MJK (c); with 7BJ6 (d); with 2VTA (e); with 3VHE (f) and with 6LVK (g)

site of the receptor molecules [57]. The plots on the left are 3D representations while those at the right are the 2D projections. The pocket areas with hydrogen bonding donors are purple while the acceptors are green. Since, MeOIstMe did not yield distinctly better binding affinities than MeOIstEt, its atomic level interactions are not presented in the figures.

The occurrences of hydrogen bonding, ionic, unfavourable, pi-related and alkyl related interactions with different amino acid residues of various proteins are presented in Table-4. In case of hydrogen bonding, the distances are also shown. Even though some interactions are unfavourable, the presence of other strong non-covalent interactions makes the complex

TABLE-4
AMINO ACID RESIDUES INVOLVED IN MAJOR INTERACTIONS WITH MeOIstEt AND DISTANCES (Å)

PDB ID	Hydrogen-bonds	Salt-bridge/others	Pi related	Alkyl related
4ASD	ASP1046 (4.17, 3.78), VAL899 (3.23)	GLU885	LEU889	LYS868, HIS1026
3MJG	MET65 (1.77), LEU93 (1.95), THR95 (1.88), ARG150 (1.83)	ARG64	GLU63, GLU97	MET65, PHE99
3MJK	ARG83 (5.12, 5.25)	LEU164	GLU166	LYS165, VAL167
7BJ6	LEU54 (2.14)	–	PHE86, PHE91	LEU57
2VTA	GLU81 (4.80), LEU83 (4.23, 5.33), ILE10 (4.32)	ILE10, ASP145	LEU134	ALA31, VAL18
3VHE	CYS919 (3.66), GLU917 (4.03)	PHE1047	LEU1035	ALA866
6LVK	GLU565 (1.88), ALA567 (1.84, 2.08)	VAL564, LEU633	ILE548, LEU633	ALA643, LEU487

stable in nature. In case of 4ASD, the key amino acid residues ASP1046, VAL899, LYS868 and GLU885 are involved and have also been reported in case of docking with compounds derived from well-known drugs [58] for cancer. In case of 3MJG protein the major interaction is with the residues MET65, LEU93, THR95 and ARG150 with short hydrogen bonding distances. Other key residues THR86 and THR88 have been reported to be involved in interaction with a different compound, indigocarpan [59]. 3MJK protein involves a residue ARG83 with weak hydrogen bonding and other interactions with GLU166, LYS165 and VAL167. However, CYS96, LYS97, SER143, HIS146, ARG148, GLU176 and CYS177 are the key residues reported with Litreol. With titerpenes the key residues are ILE38, HIS39, VAL95, LYS97, THR98, TRP120, PRO121, VAL124, ARG148, VAL152 and VAL160 [60]. None of the residues match thus pointing towards different site for docking of the small molecule. The key residue in case of 7BJ6 are LEU54, PHE86, PHE91 and LEU57 as shown in Fig. 4d. But other set of key residues GLN72, MET62, GLY58, GLN59 and VAL93 have been reported [61] for its native ligand, an isoindolinone. This is due to slight shifting of docking position by the compound. The protein 2VTA has been found to interact with the test compound with the residues VAL18, GLU81, LEU83, ILE10, ASP145, LEU134 and ALA31. All the residues are same as in its native ligand except PHE80, PHE82 and ALA144. 3VHE protein has residues CYS919 and GLU917 involved in weaker hydrogen bonding. CYS919 and LYS920 have been reported as key residues while interacting with indigocarpan in other studies [59]. In case of 6LVK, there are two amino acid residues GLU565 and ALA567 with strong hydrogen bonding (short distances) with MeOIstEt and similar residues have been reported with the native ligand. In most of the cases, the involvement of same amino acid residues suggests that the test compound is bound at the vicinity of the active site of the protein and thus may lead to its effective inhibition.

Based on the observation of interactions at the methoxy end of the compound, it can be inferred that its replacement with other larger functional groups like butoxy or phenyl rings with diverse substituents (electron withdrawing or even electron donating) may lead to stronger binding at the active pocket. Thus, the synthesis of different compounds with the same scaffold but with slight variation in substituent that favour non-covalent interactions (hydrogen bond, ionic and pi-related) with the key amino acid residues would be appropriate. The presence of donors for hydrogen bond formation from the residues of the protein in most of the cases suggests the inclusion of functional group with electronegative elements. This proposition is in accordance to the composition of the FDA approved drug imatinib, which contains multiple nitrogen atoms and has long molecular structure. A trial and error method or virtual screening (pharmacophore modeling) of a library of compounds with multiple types of substituent that may fulfill this criteria may usher to a better lead candidate than some of the control drugs.

Conclusion

Two thiosemicarbazones, MeOIstEt and MeOIstMe were synthesized and characterized by various spectral techniques.

They were tested for anticancer activity *in vitro* in different cancer cell lines like A549, MCF-7 and A431. Moderate anticancer activity with IC_{50} values in the range of 6.59-36.49 μM were obtained. Also, the anticancer properties of two test compounds were investigated *in silico* by various computational methods using either free software or online servers. One of these compounds, MeOIstEt hint of being biologically active and showed better binding affinity than one FDA approved drug from flexible receptor molecular docking calculations in a hydrated environment. Atomic level non-covalent interactions were determined in the receptor-ligand complexes and drug likeness along with ADMET predictions made using different programs showed acceptable properties. The compounds require further *in vitro* experiments (different cell lines) and could be subjected to further *in vivo* trials. Further functionalization of the test compounds with suitable groups leading to even better binding with the target receptor may help in improving the efficacy and effectiveness of the proposed compound as a good cancer drug. In order to determine the stability of complex, the trajectory of the ligand inside the active site, its RMSD and free energy needs to be analyzed. It requires molecular dynamics simulation of the complex with production run of 200 nanoseconds or longer and is currently being pursued. This work shows that computational technique could be synergistically used with experiments for better insights and proper justification in the search of therapeutics against different diseases.

CONFLICT OF INTEREST

The authors declare that there is no conflict of interests regarding the publication of this article.

REFERENCES

1. H.A. Mahdy, M.K. Ibrahim, A.M. Metwaly, A. Belal, A.B.M. Mehany, K.M.A. El-Gamal, A. El-Sharkawy, M.A. Elhendawy, M.M. Radwan, M.A. Elsholy and I.H. Eissa, *Bioorg. Chem.*, **94**, 103422 (2020); https://doi.org/10.1016/j.bioorg.2019.103422

2. V.R. Solomon, C. Hu and H. Lee, *Bioorg. Med. Chem.*, **17**, 7585 (2009); https://doi.org/10.1016/j.bmc.2009.08.068

3. R.L.D. Havrylyuk, B. Zimenkovsky, O. Vasylenko, A. Gzella and R. Lesyk, *J. Med. Chem.*, **55**, 8630 (2012); https://doi.org/10.1021/jm300789g

4. R. Sribalan, G. Banuppriya, M. Kirubavathi and V. Padmini, *J. Mol. Struct.*, **1175**, 577 (2019); https://doi.org/10.1016/j.molstruc.2018.07.114

5. A. Cane, M.C. Tournaire, D. Barritault and M. Crumeyrolle-Arias, *Biochem. Biophys. Res. Commun.*, **276**, 379 (2000); https://doi.org/10.1006/bbrc.2000.3477

6. N.M. Evdokimov, I.V. Magedov, D. McBrayer and A. Kornienko, *Bioorg. Med. Chem. Lett.*, **26**, 1558 (2016); https://doi.org/10.1016/j.bmcl.2016.02.015

7. K.L. Vine, J.M. Locke, M. Ranson, S.G. Pyne and J.B. Bremner, *Bioorg. Med. Chem.*, **15**, 931 (2007);
https://doi.org/10.1016/j.bmc.2006.10.035

8. N. Karali, *Eur. J. Med. Chem.*, **37**, 909 (2002);
https://doi.org/10.1016/S0223-5234(02)01416-2

9. B. Shakya, N. Shahi, F. Ahmad, P.N. Yadav and Y.R. Pokharel, *Bioorg. Med. Chem. Lett.*, **29**, 1677 (2019);
https://doi.org/10.1016/j.bmcl.2019.04.031

10. N.V.Z. Juranic, F. Anastasova, I. Juranic, T. Stanojkovic and S. Radulovic, *J. Exp. Clin. Cancer Res.*, **3**, 317 (1999).

11. H. Pervez, N. Manzoor, M. Yaqub, A. Khan, K.M. Khan, F.H. Nasim and M.I. Choudhary, *Lett. Drug Des. Discov.*, **7**, 102 (2010);
https://doi.org/10.2174/157018010790225840

12. S. Saranya, J. Haribabu, V.N. Vadakkedathu Palakkeezhillam, P. Jerome, K. Gomathi, K.K. Rao, V.H.H. Surendra Babu, R. Karvembu and D. Gayathri, *J. Mol. Struct.*, **1198**, 126904 (2019);
https://doi.org/10.1016/j.molstruc.2019.126904

13. A.Q. Ali, S.G. Teoh, A. Salhin, N.E. Eltayeb, M.B. Khadeer Ahamed and A.M.S.A. Majid, *Spectrochim. Acta A Mol. Biomol. Spectrosc.*, **125**, 440 (2014);
https://doi.org/10.1016/j.saa.2014.01.086

14. K.N. Aneesrahman, K. Ramaiah, G. Rohini, G.P. Stefy, N.S.P. Bhuvanesh and A. Sreekanth, *Inorg. Chim. Acta*, **492**, 131 (2019);
https://doi.org/10.1016/j.ica.2019.04.019

15. M.A. Demertzis, P.N. Yadav and D. Kovala-Demertzi, *Helv. Chim. Acta*, **89**, 1959 (2006);
https://doi.org/10.1002/hlca.200690187

16. G. Munikumari, R. Konakanchi, V.B. Nishtala, G. Ramesh, L.R. Kotha, K.B. Chandrasekhar and C. Ramachandraiah, *Synth. Commun.*, **49**, 146 (2019);
https://doi.org/10.1080/00397911.2018.1546400

17. P.N. Yadav, N.K. Singh, S. Sharma, A. Krishnakumar, R.K. Choudhary, A.A. Kumbhar, R.J. Butcher and Y.R. Pokharel, *J. Inorg. Biochem.*, (2022);
https://doi.org/10.2139/ssrn.4042515

18. M. Muralisankar, S. Sujith, N.S.P. Bhuvanesh and A. Sreekanth, *Polyhedron*, **118**, 103 (2016);
https://doi.org/10.1016/j.poly.2016.06.017

19. J. Haribabu, G.R. Subhashree, S. Saranya, K. Gomathi, R. Karvembu and D. Gayathri, *J. Mol. Struct.*, **1110**, 185 (2016);
https://doi.org/10.1016/j.molstruc.2016.01.044

20. L.M. Finkielsztein, E.F. Castro, L.E. Fabian, G.Y. Moltrasio, R.H. Campos, L.V. Cavallaro and A.G. Moglioni, *Eur. J. Med. Chem.*, **43**, 1767 (2008);
https://doi.org/10.1016/j.ejmech.2007.10.023

21. N.K. Singh, S. Shrestha, N. Shahi, R.K. Choudhary, A.A. Kumbhar, Y.R. Pokharel and P.N. Yadav, *Rasayan J. Chem.*, **14**, 1600 (2021);
https://doi.org/10.31788/RJC.2021.1436341

22. A.Q. Ali, S.G. Teoh, A. Salhin, N.E. Eltayeb, M.B.K. Ahamed and A.M.S.A. Majid, *Inorg. Chim. Acta*, **416**, 235 (2014);
https://doi.org/10.1016/j.ica.2014.03.029

23. P.N. Yadav, M.A. Demertzis, D. Kovala-Demertzi, A. Castineiras and D.X. West, *Inorg. Chim. Acta*, **332**, 204 (2002);
https://doi.org/10.1016/S0020-1693(02)00710-7

24. M. Joseph, V. Suni, M.R. Prathapachandra Kurup, M. Nethaji, A. Kishore and S.G. Bhat, *Polyhedron*, **23**, 3069 (2004);
https://doi.org/10.1016/j.poly.2004.09.026

25. M.S. Çavuş, H. Yakan, H. Muglu and T. Bakir, *J. Phys. Chem. Solids*, **140**, 109362 (2020);
https://doi.org/10.1016/j.jpcs.2020.109362

26. G.A. Bain, D.X. West, J. Krejci, J. Valdés-s-Martinez, S. Hernández-Ortega and R.A. Toscano, *Polyhedron*, **16**, 855 (1997);
https://doi.org/10.1016/S0277-5387(96)00323-3

27. C. Balachandran, J. Haribabu, K. Jeyalakshmi, N.S.P. Bhuvanesh, R. Karvembu, N. Emi and S. Awale, *J. Inorg. Biochem.*, **182**, 208 (2018);
https://doi.org/10.1016/j.jinorgbio.2018.02.014

28. D. Kovala-Demertzi, M. Demertzis, P.N. Yadav, A. Castiñeiras and D.X. West, *Transition Met. Chem.*, **24**, 642 (1999);
https://doi.org/10.1023/A:1006989117072

29. A.J. Abdulghani and N.M. Abbas, *Bioinorg. Chem. Appl.*, **2011**, 706262 (2011);
https://doi.org/10.1155/2011/706262

30. H. Muglu, *Res. Chem. Intermed.*, **46**, 2083 (2020);
https://doi.org/10.1007/s11164-020-04079-x

31. N.K. Singh, S. Shrestha, N. Shahi, R.K. Choudhary, A.A. Kumbhar, Y.R. Pokharel and P.N. Yadav, *Asian J. Chem.*, **33**, 557 (2021);
https://doi.org/10.14233/ajchem.2021.23004

32. A.M.S. El-Sharief, Y.A. Ammar, A. Belal, M.A.M.S. El-Sharief, Y.A. Mohamed, A.B.M. Mehany, G.A.M. Elhag Ali and A. Ragab, *Bioorg. Chem.*, **85**, 399 (2019);
https://doi.org/10.1016/j.bioorg.2019.01.016

33. R. Bhuvaneswari, M. Divya Bharathi, G. Anbalagan, G. Chakkaravarthi and K.S. Murugesan, *J. Mol. Struct.*, **1173**, 188 (2018);
https://doi.org/10.1016/j.molstruc.2018.06.109

34. U. Chaudhary, D. Dawa, I. Banerjee, S. Sharma, K. Mahiya, A. Rauf, Y.R. Pokharel and P.N. Yadav, *J. Mol. Struct.*, **1274**, 134549 (2023);
https://doi.org/10.1016/j.molstruc.2022.134549

35. E. Labisbal, A. Sousa, A. Castiñeiras, J.A. García-Vázquez, J. Romero and D.X. West, *Polyhedron*, **19**, 1255 (2000);
https://doi.org/10.1016/S0277-5387(00)00383-1

36. N.T. Akinchan, P.M. Drozdzewski and W. Holzer, *J. Mol. Struct.*, **641**, 17 (2002);
https://doi.org/10.1016/S0022-2860(02)00134-5

37. Y.H. Lu, Y.W. Lu, C.L. Wu, Q. Shao, X.L. Chen and R.N.B. Bimbong, *Spectrochim. Acta A Mol. Biomol. Spectrosc.*, **65**, 695 (2006);
https://doi.org/10.1016/j.saa.2005.12.032

38. T.D. Kühne, M. Iannuzzi, M. Del Ben, V.V. Rybkin, P. Seewald, F. Stein, T. Laino, R.Z. Khaliullin, O. Schütt, F. Schiffmann, D. Golze, J. Wilhelm, S. Chulkov, M.H. Bani-Hashemian, V. Weber, U. Borštnik, M. Taillefumier, A.S. Jakobovits, A. Lazzaro, H. Pabst, T. Müller, R. Schade, M. Guidon, S. Andermatt, N. Holmberg, G.K. Schenter, A. Hehn, A. Bussy, F. Belleflamme, G. Tabacchi, A. Glöß, M. Lass, I. Bethune, C.J. Mundy, C. Plessl, M. Watkins, J. VandeVondele, M. Krack and J. Hutter, *J. Chem. Phys.*, **152**, 194103 (2020);
https://doi.org/10.1063/5.0007045

39. P.A. Ravindranath, S. Forli, D.S. Goodsell, A.J. Olson and M.F. Sanner, *PLOS Comput. Biol.*, **11**, e1004586 (2015);
https://doi.org/10.1371/journal.pcbi.1004586

40. W. Tian, C. Chen, X. Lei, J. Zhao and J. Liang, *Nucleic Acids Res.*, **46(no. W1)**, W363 (2018);
https://doi.org/10.1093/nar/gky473

41. H.M. Berman, *Nucleic Acids Res.*, **28**, 235 (2000);
https://doi.org/10.1093/nar/28.1.235

42. R. Board and G.C. Jayson, *Drug Resist. Updat.*, **8**, 75 (2005);
https://doi.org/10.1016/j.drup.2005.03.004

43. X. Wang, Y. Shen, S. Wang, S. Li, W. Zhang, X. Liu, L. Lai, J. Pei and H. Li, *Nucleic Acids Res.*, **45(no. W1)**, W356 (2017);
https://doi.org/10.1093/nar/gkx374

44. P.G. Wyatt, A.J. Woodhead, V. Berdini, J.A. Boulstridge, M.G. Carr, D.M. Cross, D.J. Davis, L.A. Devine, T.R. Early, R.E. Feltell, E.J. Lewis, R.L. McMenamin, E.F. Navarro, M.A. O'Brien, M. O'Reilly, M. Reule, G. Saxty, L.C.A. Seavers, D.M. Smith, M.S. Squires, G. Trewartha, M.T. Walker and A.J.-A. Woolford, *J. Med. Chem.*, **51**, 4986 (2008);
https://doi.org/10.1021/jm800382h

45. I. Kuriwaki, M. Kameda, H. Hisamichi, S. Kikuchi, K. Iikubo, Y. Kawamoto, H. Moritomo, Y. Kondoh, Y. Amano, Y. Tateishi, Y. Echizen, Y. Iwai, A. Noda, H. Tomiyama, T. Suzuki and M. Hirano, *Bioorg. Med. Chem.*, **28**, 115453 (2020);
https://doi.org/10.1016/j.bmc.2020.115453

46. L. Mazumder, M.R. Hasan, K. Fatema, M.Z. Islam and S.K. Tamanna, *BioMed Res. Int.*, **2022**, 4302625 (2022);
https://doi.org/10.1155/2022/4302625

47. C. Colovos and T. Yeates, *Protein Sci.*, **2**, 1511 (1993);
https://doi.org/10.1002/pro.5560020916

48. D.K.A. Mohan and P. Gangwar, *World J. Pharm. Res.*, **2**, 1114 (2013).

49. B.Z. Sibuh, P.K. Gupta, P. Taneja, S. Khanna, P. Sarkar, S. Pachisia, A.A. Khan, N.K. Jha, K. Dua, S.K. Singh, S. Pandey, P. Slama, K.K. Kesari and S. Roychoudhury, *Biomedicines*, **9**, 1375 (2021);
https://doi.org/10.3390/biomedicines9101375

50. S. Kim, J. Chen, T. Cheng, A. Gindulyte, J. He, S. He, B.A. Shoemaker, Q. Li, P.A. Thiessen, B. Yu, L. Zaslavsky, J. Zhang and E.E. Bolton, *Nucleic Acids Res.*, **49(no. D1)**, D1388 (2021);
https://doi.org/10.1093/nar/gkaa971

51. K. Tallapragada, J. Chewning, D. Kombo and B. Ludwick, *J. Cheminform.*, **4**, 1 (2012);
https://doi.org/10.1186/1758-2946-4-1

52. B. Schiffrin, S.E. Radford, D.J. Brockwell and A.N. Calabrese, *Protein Sci.*, **29**, 1851 (2020);
https://doi.org/10.1002/pro.3902

53. G. Xiong, Z. Wu, J. Yi, L. Fu, Z. Yang, C. Hsieh, M. Yin, X. Zeng, C. Wu, A. Lu, X. Chen, T. Hou and D. Cao, *Nucleic Acids Res.*, **49(no. W1)**, W5 (2021);
https://doi.org/10.1093/nar/gkab255

54. R. Al-Jarf, A.G.C. de Sá, D.E.V. Pires and D.B. Ascher, *J. Chem. Inf. Model.*, **61**, 3314 (2021);
https://doi.org/10.1021/acs.jcim.1c00168

55. J. Blaney, *J. Comput. Aided Mol. Des.*, **26**, 13 (2012);
https://doi.org/10.1007/s10822-011-9518-x

56. M. Batool, B. Ahmad and S. Choi, *Int. J. Mol. Sci.*, **20**, 2783 (2019);
https://doi.org/10.3390/ijms20112783

57. D. Systèmes, BIOVIA Discovery Studio Visualizer, San Diego: Dassault Systèmes (2020); https://3ds.com/products-services/biovia/products

58. N.A.A.M. Aziz, R.F. George, K. El-Adl and W.R. Mahmoud, *RSC Adv.*, **12**, 12913 (2022);
https://doi.org/10.1039/D2RA01119K

59. S.K. Paramashivam, K. Elayaperumal, B. Natarajan, M. Ramamoorthy, S. Balasubramanian and K.N. Dhiraviam, *Bioinformation*, **11**, 73 (2015);
https://doi.org/10.6026/97320630011073

60. A.B. Mahajanakatti, G. Murthy, N. Sharma and S. Skariyachan, *Interdiscip. Sci.*, **6**, 13 (2014);
https://doi.org/10.1007/s12539-014-0170-8

61. G. Chessari, I.R. Hardcastle, J.S. Ahn, B. Anil, E. Anscombe, R.H. Bawn, L.D. Bevan, T.J. Blackburn, I. Buck, C. Cano, B. Carbain, J. Castro, B. Cons, S.J. Cully, J.A. Endicott, L. Fazal, B.T. Golding, R.J. Griffin, K. Haggerty, S.J. Harnor, K. Hearn, S. Hobson, R.S. Holvey, S. Howard, C.E. Jennings, C.N. Johnson, J. Lunec, D.C. Miller, D.R. Newell, M.E.M. Noble, J. Reeks, C.H. Revill, C. Riedinger, J.D. St. Denis, E. Tamanini, H. Thomas, N.T. Thompson, M. Vinkovic, S.R. Wedge, P.A. Williams, N.E. Wilsher, B. Zhang and Y. Zhao, *J. Med. Chem.*, **64**, 4071 (2021);
https://doi.org/10.1021/acs.jmedchem.0c02188